Colour Adjustment of Aerial Images from 2000–3000 m Altitude: Empirical Normalisation using Large Ground Colour Targets

Ivar Oveland[1], Steven Le Moan[2]

[1] The Norwegian Mapping Authority, Kristiansand, Norway - ivar.oveland@kartverket.no
[2] Colourlab, Norwegian University of Science and Technology, Gjøvik, Norway - steven.lemoan@ntnu.no

Keywords: Aerial imagery, radiometric normalisation, colour calibration, CIELAB, empirical correction, ground targets

Abstract

High-altitude aerial image national mosaics often exhibit visible colour and tone differences caused by atmospheric variability, illumination changes, sensor differences and post-processing workflows. These radiometric inconsistencies negatively influence both visual quality and the comparability of image data across sensors, time and campaigns. This work presents an empirical two-step colour adjustment and radiometric normalisation method for imagery acquired from 2000–3000 m altitude using a large multi-colour ground target designed to provide stable, spatially robust reference statistics. Field reflectance values are measured with a handheld spectrometer and converted to CIELAB coordinates. A global 3D similarity (Helmert) transform aligns measured image colours to ground-truth CIELAB values, followed by local residual chromatic correction using inverse distance weighting. Experiments on aerial datasets demonstrate that the method significantly reduces colour discrepancies at the calibration site.

1. Introduction

Aerial images captured from fixed-wing aircraft are essential for national mapping, land administration, topographic modelling, and environmental monitoring. Operating altitudes of 2–3 km enable centimetre-level ground sampling distances, but still leave imagery affected by atmospheric scattering, illumination variability, adjacency effects and camera-related radiometric nonuniformity (Vermote et al., 1997, Richter et al., 2006). When orthophoto tiles from multiple acquisitions are mosaicked, these effects lead to visible seams, spatially inconsistent colour appearance and reduced interpretability (Collings et al., 2011, Honkavaara and Khoramshahi, 2018).

Radiometric harmonisation is increasingly important due to evolving acquisition practices: multi-vendor camera fleets, hybrid panchromatic–RGB–NIR optical systems, and long-term national mapping programs relying on imagery collected across multiple years, seasons and operators (Honkavaara and Khoramshahi, 2018). Although radiative transfer–based atmospheric correction tools such as 6S (Vermote et al., 1997, Wilson, 2013) and MODTRAN (Callieco and Dell'Acqua, 2011) exist, their application requires accurate and contemporaneous atmospheric measurements which are rarely obtained for manned airborne campaigns due to cost, logistics, and lack of sensor payload support. As a result, mapping agencies often rely on empirical post-hoc tonal adjustment. Recent advances in radiometric block adjustment can greatly improve spatial tonal consistency (Collings et al., 2011, Honkavaara and Khoramshahi, 2018), but they enforce relative radiometric similarity, not a direct physical linkage to stable reference reflectance.

Ground-based vicarious calibration offers an alternative path. Satellite calibration sites, permanent RadCalNet stations and large artificial targets are widely used for orbital sensor validation (Bouvet et al., 2019, Cantrell and Christopherson, 2024). However, for aerial missions, traditional white/gray reference panels are usually too small, subtending only a few pixels at 2–3 km altitude, limiting extraction of reliable statistics and complicating automated detection (Smith and Milton, 1999, Shin et al., 2020). Furthermore, small panels pose operational burdens, are sensitive to soiling, orientation, and Bidirectional Reflectance Distribution Function (BDRF) effects, and offer limited colour diversity, restricting their use for chromatic calibration in combination with hyperspectral camera (Ban and Kim, 2021).

To our knowledge, no published work has demonstrated operational radiometric normalisation for high-altitude manned aircraft imagery using a large multi-colour ground target that provides dozens of pixels per patch, supports full-colour calibration, and enables statistically robust empirical colour mapping in CIELAB space. This research gap is critical because mapping authorities increasingly require long-term radiometric stability, lifelike colour appearance, and minimised inter-flight tonal inconsistencies.

This study has developed and evaluated a practical workflow for empirical colour adjustment using a custom-designed large ground target, combining (1) a global Helmert transform and (2) local chromatic residual correction using inverse distance weighting (IDW). The approach is designed for real-world survey operations rather than laboratory or campaign-specific research settings.

1.1 Related Work

Radiometric normalisation approaches can be grouped into: (1) physically based atmospheric correction, (2) relative image-based harmonisation, and (3) vicarious calibration using ground targets.

(1) Physically based atmospheric correction. Atmospheric radiative transfer models such as 6S and Py6S (Vermote et al., 1997, Wilson, 2013) estimate surface reflectance from top-of-atmosphere measurements but require accurate aerosol optical depth, water vapour, spectral response and solar geometry.

Such parameters are rarely acquired alongside large-format aerial mapping operations, limiting practicality.

(2) Relative image-based harmonisation. Techniques such as histogram matching, dark-object subtraction (Chavez Jr, 1988), radiometric block adjustment (Chandelier et al., 2009), and recent radiometric-invariant bundle models (Honkavaara and Khoramshahi, 2018) produce visually consistent mosaics but do not link imagery to stable colour ground truth. Thus, long-term monitoring and cross-sensor standardisation remain challenging.

(3) Vicarious calibration using ground targets. The empirical line method (Smith and Milton, 1999) enables reflectance-based calibration using ground targets but typically requires multiple well-characterised panels spanning the brightness range. UAV-focused studies show progress towards automation (Shin et al., 2020, Ban and Kim, 2021) but operate at tens–hundreds of metres altitude, where small targets map to many pixels. Global satellite calibration infrastructures (e.g., RadCalNet) achieve high accuracy but are beyond scope for routine aerial surveys (Bouvet et al., 2019, Cantrell and Christopherson, 2024).

Our contribution differs by deploying a multi-colour, metre-scale ground reference enabling full-colour empirical normalisation tailored for high-altitude aerial photogrammetry, bridging the gap between UAV vicarious calibration and satellite-oriented infrastructures.

2. Materials and Methods

2.1 Study design and workflow overview

This study evaluates an empirical workflow for colour normalisation of high-altitude aerial imagery using a large multi-colour ground target. Field-measured CIELAB reference values are matched to corresponding image patch colours, followed by a global alignment using a three-dimensional similarity (Helmert) transform. Residual chromatic errors are then corrected locally using IDW in CIELAB space. The corrected image is evaluated against the ground references and through visual inspection.

Field measurements on the ground target provide a set of reference colours $\{\mathbf{L}^*\mathbf{a}^*\mathbf{b}^*{}_{\text{field}}\}$, while the corresponding patch colours in the aerial image provide $\{\mathbf{L}^*\mathbf{a}^*\mathbf{b}^*{}_{\text{image}}\}$. These two sets of coordinates are first related using a three-dimensional similarity (Helmert) transform, which globally corrects for translation, rotation and uniform scaling in CIELAB space. The residual colour differences after this global step are then modelled locally in the chromatic a–b plane using IDW interpolation, based on the remaining errors at the patch locations in the CIELAB colour space.

The overall procedure thus consists of:

1. extracting representative CIELAB coordinates for each patch in the field measurements (in situ) and in the aerial image;
2. using the result from point 1 to estimating a 3D similarity transform in CIELAB space from image colour to field colour coordinates;
3. applying this transform to all image pixels;
4. extracting representative CIELAB coordinates for each patch in the in the 3D similarity transformed aerial image;
5. estimating local residual vectors in the a–b plane for each patch; and
6. applying the residual corrections to the chromatic coordinates of all image pixels using IDW and the residual vectors for the three closest patches, all performed in the CIELAB colour space.

We emphasise that this is an empirical colour normalisation, not a full physical atmospheric correction to surface reflectance.

2.2 Helmert transformation

The Helmert transformation is commonly used in geodesy to convert between different coordinate reference frames. This mathematical method estimates rotation, translation and scale to transform coordinates between two coordinate systems. In this study we use the same type of similarity transform but applied to colour coordinates rather than to geospatial coordinates.

All processing in this step is done in the CIELAB colour space. All conversion between colour spaces is done with built-in functions in Matlab. For the relatively small colour differences observed in this project, Euclidean distance in CIELAB (ΔE^*_{ab}) is assumed to be an adequate approximation to perceptual colour difference . We treat CIELAB coordinates as 3D vectors (L^*, a^*, b^*) and estimate a similarity transform of the form

$$\mathbf{x}_{\text{field}} = s\,\mathbf{R}\,\mathbf{x}_{\text{image}} + \mathbf{t},$$

where s is a global scale factor, $\mathbf{R}$ is a 3×3 rotation matrix and $\mathbf{t}$ is a translation vector in CIELAB space. A positive scale factor increases the overall spread of colours around the origin in CIELAB, whereas the rotation accounts for cross-coupling between the three axes.

In this study the transformation is estimated from paired lists of colour coordinates. The first list represents the measured colour in the field, and the second list is the corresponding colour measured in the image. The difference between the two lists is illustrated in Figure 3. The Helmert transformation (Wasmeier, 2025) is used to transform the image colours so that, in a least-squares sense, they best match the field observation colours. We note that this similarity mapping is an empirical model of the combined camera, atmospheric and processing effects in CIELAB space; it is not a physically based device characterisation.

2.3 Local residual correction using Inverse Distance Weighting

The Helmert transformation provides a global best-fit alignment between image and field colours. A natural consequence is that residual colour errors remain, as illustrated in Figure 4. These errors can vary with chromaticity and lightness. In CIELAB space the relationship between input and output colours can be considered nonlinear, reflecting combined contributions from Rayleigh and Mie scattering, atmospheric absorption, camera behaviour, post-processing operations and uncertainties in the in situ measurements.

There are different methods to correct for such nonlinear effects. Kriging (Oliver and Webster, 1990), also known as Gaussian process regression, is a well-known method that interpolates between in situ measurements. Other methods include Bayes linear statistics, multivariate interpolation, nonparametric regression, radial basis function interpolation, space mapping, information field theory, collocation and inverse distance weighting. In this study an inverse distance weighting method is chosen as a simple and transparent way to model local residuals around the calibration colours.

Using the image after the Helmert transformation, the colour distance between the in situ patch values and the corresponding pixel values in the transformed image is estimated. For a given patch, the CIELAB distance is defined as:

$$d_{\text{patch}} = \sqrt{(a_{\text{in situ}} - a_{\text{image}})^2 + (b_{\text{in situ}} - b_{\text{image}})^2}.$$

For each pixel in the image, the colour distance to each calibration patch is computed in the CIELAB colour space. The three closest patches in the CIELAB colour space are identified. The total distances S to the three closest patches are calculated. Let the distances to these patches be denoted by $d_{(1)}, d_{(2)}, d_{(3)}$, where:

$$S = d_{(1)} + d_{(2)} + d_{(3)}.$$

A weight V_k for each of the three closest patches is computed as:

$$V_k = \frac{1}{d_{(k)}/S}, \qquad k = 1, 2, 3.$$

The normalised weight w_k is then given by:

$$w_k = \frac{V_k}{V_1 + V_2 + V_3}, \qquad k = 1, 2, 3.$$

Each patch has an associated CIELAB delta vector defined as:

$$\delta_{i_k} = \begin{bmatrix} \delta_{i_k,A} \\ \delta_{i_k,B} \end{bmatrix} = \begin{bmatrix} a_{\text{image}} - a_{\text{in situ}} \\ b_{\text{image}} - b_{\text{in situ}} \end{bmatrix}, \qquad k = 1, 2, 3.$$

The corrected CIELAB components for each pixel are computed as:

$$A_{\text{new}} = A_{\text{old}} + (w_1\, \delta_{i_1,A} + w_2\, \delta_{i_2,A} + w_3\, \delta_{i_3,A})\,,$$

$$B_{\text{new}} = B_{\text{old}} + (w_1\, \delta_{i_1,B} + w_2\, \delta_{i_2,B} + w_3\, \delta_{i_3,B})\,.$$

The IDW method does not assume any specific statistical model or random process, which makes it simple to implement but limits its ability to capture large-scale global trends. The method is sensitive to clustering of points, which can introduce bias if calibration patches are unevenly distributed. In our implementation, the residual correction is applied only to the two chromatic dimensions a^* and b^*, leaving L^* unchanged. This design choice is motivated by the observation that the largest systematic errors in our data are chromatic, whereas variations in L^* are strongly influenced by local illumination, shadows and potential saturation effects.

2.4 User questionnaire

To determine which radiometric and appearance-related qualities are most useful to expert users, a short questionnaire was conducted during a national geospatial conference in Norway (Geoforum, 2024). Participants are typically professional users of geospatial information from the private, municipal and government sectors. The questionary had 7 questions (5 multiple-choice and 2 in free text form). In total, 63 responses were received. 83% of respondents reported using orthophotos weekly and 73% used them for work-related purposes. In one question, participants were asked to rate the importance of different image attributes: looks nice, lifelike colours, radiometric accuracy, radiometric stability, geometric resolution, shadows, cloud free and geometric accuracy.

The results presented in Table 1, showed that radiometric accuracy was the lowest ranked attribute, whereas shadows were ranked as the most important. Lifelike colours and radiometric stability received higher average scores within the radiometry-related topics.

Topics	score in % of a sample of 63		
	unimportant	neutral	important
looks nice	18	14	69
lifelike colours	8	9	83
radiometric accuracy	16	38	46
radiometric stability	18	11	71
ground resolution	8	8	84
shadows	6	7	87
cloud free	8	13	79
geometric accuracy	10	15	75

Table 1. Ranking of selected qualities in aerial images.

These findings motivate our focus on methods that improve visual consistency and colour stability across campaigns, rather than solely targeting absolute radiometric accuracy.

2.5 Ground target design and field reference measurements

The ground target is printed on a PVC banner with a total size of 11.5 × 6.1 m as shown in Figure 1. PVC was chosen due to its availability and the ability to print large surfaces. The banner consists of 18 different colours patches, each 1.5 × 1.5 m. The Gretag Macbeth ColourChecker (McCamy et al., 1976) was used as the basis for the patch design, with modifications to reduce the number of patches while preserving full hue coverage. The surface of the PVC banner appears matte.

The design was created for a pansharpening camera with a ratio of 1:3 and an image resolution ground sample distance (GSD) of 0.1 m. At this resolution the colour cameras have a GSD of 0.3 m. This theoretically results in 5 colour pixels and 15 pansharpening pixels within each patch. All measurements were calculated by averaging the 3×3 center pansharpening pixels of the patches. With this planned ratio, each patch covers several colour pixels in the pansharpened imagery, providing the possibility to derive stable statistics for each patch rather than relying on single pixels. By performing the colour measurements close to the centre of each patch, we reduce the impact of neighbouring colours on the field measurements, although some

spatial mixing in the aerial images remains unavoidable. Due to its large size, it was difficult to straighten the patches completely flat, resulting in small bumps that created minor shadowed areas. During the colour measurements, these shadowed areas were avoided as much as possible. Together with the averaging of the 3×3 measurements, this is assumed to reduce the impact of these effects.

The ground target patches were measured with a portable colour spectrometer called Spectro 1 Pro (Variable Inc., Chattanooga, USA). According to the manufacturer, the inter-instrument agreement is on the order of 0.22 ΔE in average with maximum 0.75 ΔE under controlled conditions (Variable, Inc., 2022). ΔE is the euclidean distances in the CIElab colour space. The instrument uses a full-spectrum LED light source. The measurements were taken with a 10° standard observer and illuminant D65, which simulates noon daylight with correlated colour temperature of approximation 6504 Kelvin. Three measurements were taken and averaged for each colour patch. The instrument is calibrated against ceramic tiles. Measurements are taken by placing the instrument directly on the surface to minimise the influence of the ambient light. The measurements were performed on 8 April 2025.

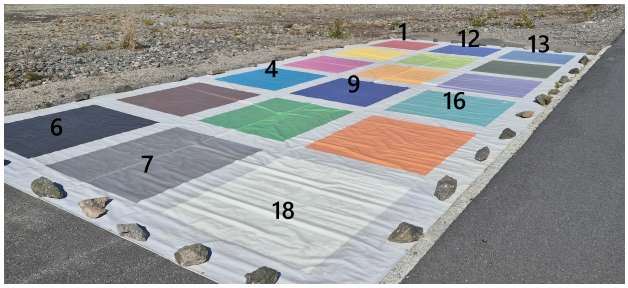

Figure 1. Ground target colour patches with numbering.

2.6 Aerial imagery and preprocessing

The aerial images used in this study were collected by Field Geospatial AS (Field Geospatial AS, 2025) with a planned ground sample distance of 0.1 meter. The camera was a UltraCam Eagle Mark 3 from the manufacture Vexcel Imaging GmbH. The image was post processed with the manufactures software UltraMap v. 6.4.0.1. The camera has four colour bands (RGB NIR) and use pan-sharpening technique with a pansharpening ratio of 1:3.

The images were captured on 6 April 2025 with an overlap in flight direction of 80% . The image in which the ground target colour patch was closest to the image center was selected. The location of the colour patches in relation to the center of the image is shown in Figure 2. The export from Ultramap was performed with neutral colour adjustment. The analyses were performed on an 8 bit Ultramap level 3 image (includes pansharpening).

3. Results

This study presents a method to adjust high-altitude aerial imagery by using a large custom-designed ground colour target as an external empirical reference. To test the method the process is applied to the original image shown in Figure 7. All adjustments are done in the CIELAB colour space with illuminant D65 as the reference white used to compute the field and image CIELAB coordinates.

Figure 2. Shows the full image used in the study and the location of the ground target patches marked with a blue rectangle.

3.1 Discrepancy between aerial and field colours

The starting point and colour differences between the in situ measurements and the measured colours in the original image are presented in the CIELAB colour space in Figure 3.

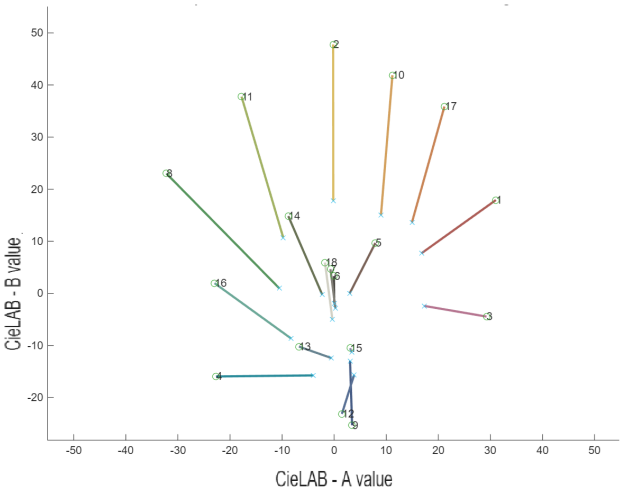

Figure 3. Differences between field measurements and the colours in the original image, visualised in the CIELAB colour space. ”o” shows the in situ colour and ”x” shows the corresponding colour in image

3.2 Effect of the Helmert transform

The first step in the colour adjustment is the Helmert transform. It corrects for the overall rotation, translation and scale in all three dimensions in the CIELAB colour space, providing a global colour normalisation. The result is shown in Figure 4 and Figure 6.

3.3 Effect of the IDW residual correction

The last step is the IDW using the three nearest in situ observations in the a–b plane. This step is applied only to the two chromatic dimensions a^* and b^*. The result is visualised in the CIELAB colour space in Figure 5 and in the sRGB colour space in Figure 8.

3.4 Quantitative error summary

The final result shown in Figure 8 is tested against the in situ measurements. By calculating the Euclidean distance in the

This contribution has been peer-reviewed. The double-blind peer-review was conducted on the basis of the full paper.
https://doi.org/10.5194/isprs-annals-XI-1-2026-337-2026 | © Author(s) 2026. CC BY 4.0 License.

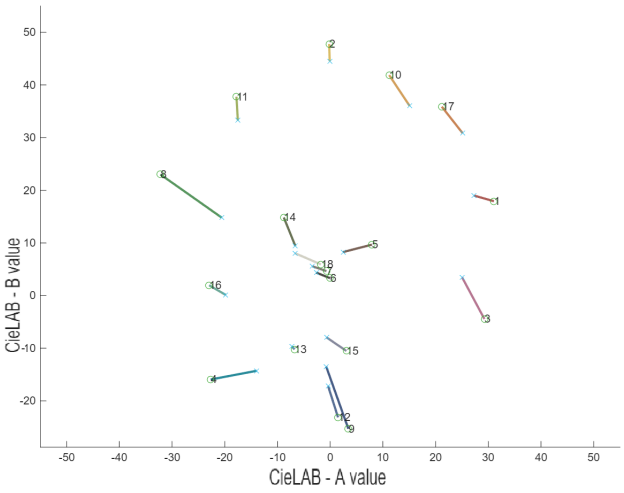

Figure 4. Differences between field-measured colours and image-derived colours after the Helmert transformation, visualised in CIELAB colour space. Circles (“o”) represent the in situ colour measurements, while crosses (“x”) indicate the corresponding colours extracted from the image.

CIELAB colour space, we can express the colour differences with (ΔE^*) , shown in Figure 9. The maximum (ΔE^*) in the a-b plane is 1.8 (ΔE^*) estimated for colour patch number 14, while the average is 0.89 (ΔE^*). The maximum value in the full (L^*, a^*, b^*) is 15.6 (ΔE^*). Offset values in the range from 0 to 1 are considered not perceptible, while a (ΔE^*) larger than approximately 2 is considered to be clearly visible under standard viewing conditions.

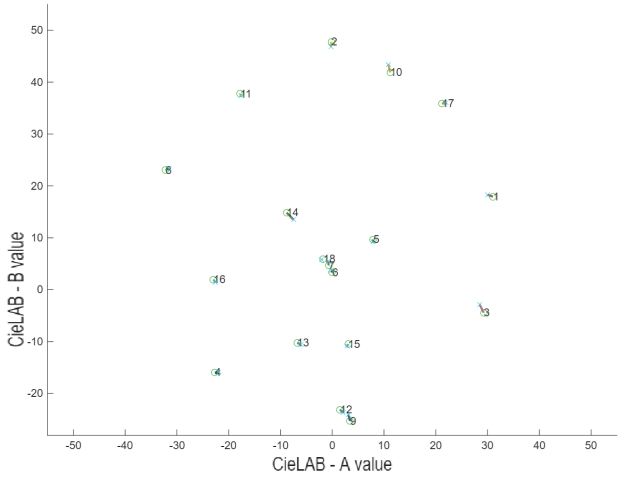

Figure 5. Differences between field-measured colours and the final adjusted image-derived colours. Circles (“o”) represent the in situ colour measurements, while crosses (“x”) indicate the corresponding colours extracted from the image.

3.5 Luminance behaviour

The evolution of the L^* values is shown in Figure 6. As expected, the L^* values do not change after the IDW transformation, since this step involves only the two chromatic dimensions. From Figure 6 it is apparent that the white, grey and black patches (patch numbers 6,7,18) exhibit large variations in L^*, especially the white patch (number 18), which suggests that luminance-related effects (e.g. haze, exposure, potential saturation and potential error in the in situ measurements) are not fully addressed by the present method.

4. Discussion

4.1 How many colour patches are needed?

The required number of patches will vary depending on the types and magnitudes of radiometric influences that affect the imagery. In the pre-study of the project, a minor selection of colour patches was tested. The result showed that the ability to adjust for nonlinear effects was limited with few colour patches. A larger number of calibration colour patches increase the ability to model complex, nonlinear distortions in colour space, but also increases the physical size and deployment effort of the target. Typical effects that gives nonlinear effects are atmospheric effects, but also the image post processing of the images were manual colour adjustments is significant source to nonlinear effects. In the pre-study there were indications that post-processing has a large influence on the deviation relative to the in situ measurements.

In the present design, 18 colour patches were chosen as a compromise between coverage of the CIELAB space and practical constraints on banner size and handling. The patches include neutrals (white, grey and black) as well as a selection of chromatic colours spanning different hues and saturations. This distribution provides sufficient sampling for the similarity transform and the local residual correction used here. A more systematic optimisation of patch number and placement, for example using experimental design techniques in CIELAB space, is left for future work.

4.2 National mosaic and radiometric stability

The survey presented in the Table 1 shows that users place greater importance on the visual quality of aerial images than on strict radiometric accuracy. At the same time, users expect aerial imagery from different projects to maintain consistent colour characteristics. This consistency ensures that a national mosaic assembled from multiple aerial photo projects appears homogeneous, with minimal visible boundaries between the datasets. Currently, this is not the case. Significant colour differences between aerial photo projects are still common. In Figure 10, three different previous projects from the national orthophoto mosaic are shown, clearly revealing the transitions between the projects. The collections from 2021 and 2024 were produced by the same provider and 2022 from another company. The images were captured during different stages of the growing season. However, the greatest source of variation is likely introduced during post-processing, where experience-based adjustments are applied without objective criteria to guide the manually chosen colour settings.

To ensure consistency across projects, certain factors must be corrected so that their influence on images is as uniform as possible from project to project. These include atmospheric and general weather conditions, pollution, and the sun angle, which varies with the date and time of day. Instrument-related factors, such as the physical camera, its settings during image capture and post processing, should be carefully performed.

At the same time, specific environmental characteristics should be preserved in the images, as they provide essential context and information. These include soil and surface moisture, snow

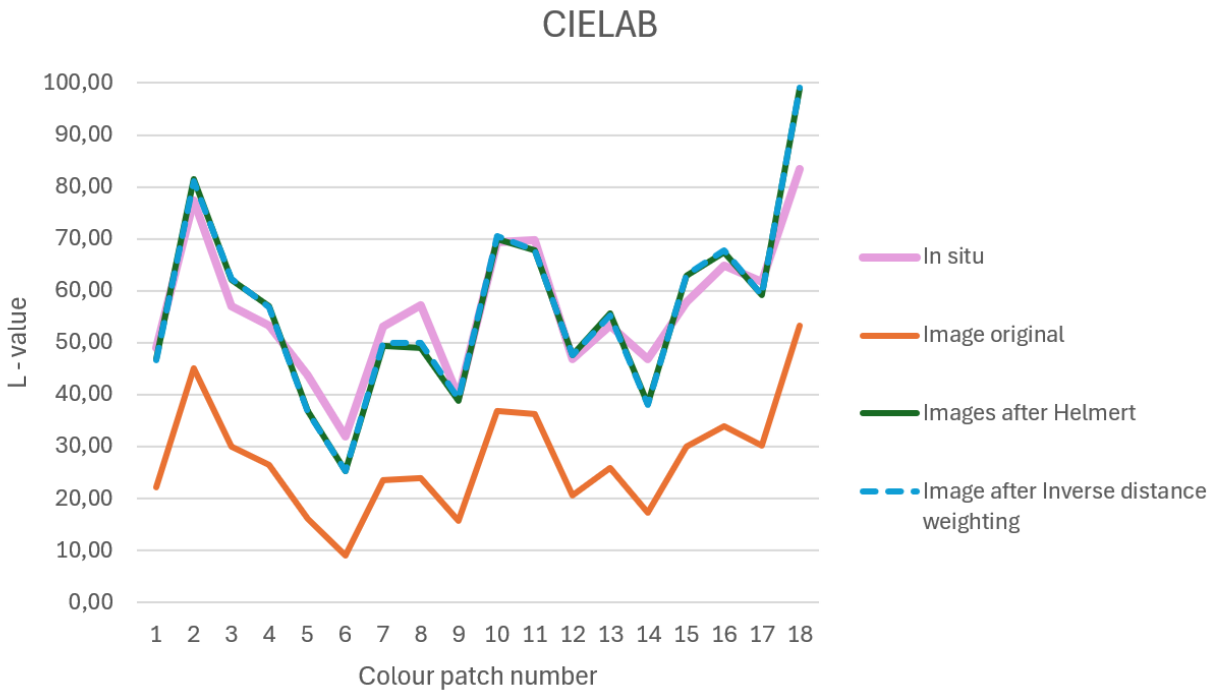

Figure 6. L^* values for the various processing steps, visualised in the CIELAB colour space.

Figure 7. Original image (subset).

Figure 8. Final colour-adjusted image (same subset as Figure 7).

conditions, the growing season, and general seasonal variations. By controlling technical and external variables while maintaining key environmental features, images can accurately represent site conditions and remain comparable across projects.

4.3 Correction grid to reduce the risko of gamut

The Helmert transformation and the subsequent residual correction can be summarised into a single look-up operation by precomputing a three-dimensional correction grid. The corrections can be stored as a three-layer GeoTIFF image. Each voxel of this 3D image represents an adjustment vector in CIELAB space, which can be applied to the corresponding range of (L^*, a^*, b^*) values.

A three-dimensional correction grid has two practical advantages. First, it decouples the calibration step from the application step: once the grid has been estimated from the ground target, it can be reused to process all images acquired during the flight mission. Second, the GeoTIFF format integrates naturally into existing geospatial workflows. However, the approach assumes that the mapping between image colours and field measurements is sufficiently smooth so that interpolation in the correction grid does not introduce artifacts.

The CIELAB colour space covers all visible colours to the human eye, but the sRGB colour space (used by monitors and images) covers a smaller subset, also referred to the sRGB gamut. When converting Lab values to sRGB, some Lab colours can fall outside the sRGB gamut. These out-of-gamut colours cannot be represented correctly in sRGB, so conversion may produce invalid values. This happens if the sRGB components are below 0 or above 255. To use the colours in standard images, these values must be mapped back into the sRGB gamut by clipping or applying a gamut-mapping method that reduces sat-

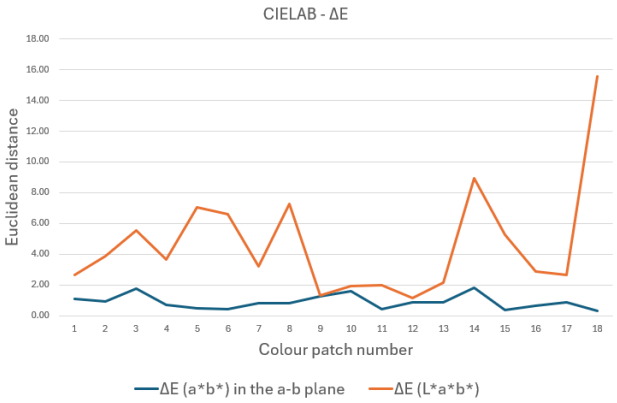

Figure 9. CIELAB (ΔE^*_{ab}) and (ΔE^*_{Lab}) for the adjusted image.

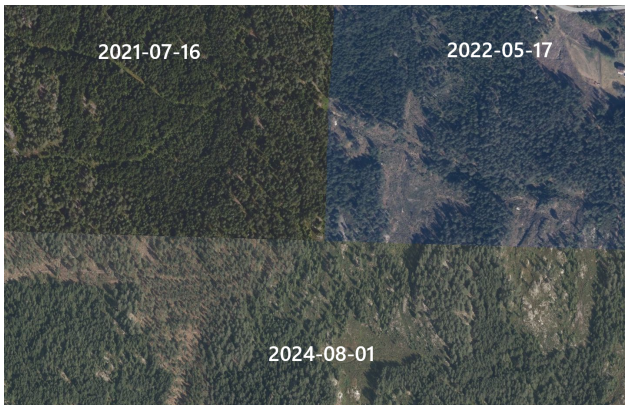

Figure 10. National mosaic made from multiple projects.

uration while preserving appearance as much as possible. Figure 11 illustrate an example of gamut and using a correction grid in one operation will reduce the risk of gamut due to multiple colour space translations.

Figure 11. Colour adjusted image with gamut.

Another factor that can reduce the risk of gamut issues is increasing the precision of the colour representation. This can be achieved by using 16-bit images instead of the 8-bit format used in this study. Higher bit depth also has the potential to improve both the transformation and the IDW process.

5. Conclusions and Outlook

The study has shown that it is possible to empirically adjust the colours of aerial images so that they better match field measurements on a large ground target. The presented method is based on techniques often used in geodesy, but instead of using geographic coordinates, it uses colour coordinates defined in the CIELAB colour space. The method is divided into two steps, where the first step corrects for mean offset, scaling and rotation in the CIELAB colour space using a standard Helmert transformation commonly employed in land survey and geodetic operations. This step provides a global colour normalisation that accounts for the combined effect of camera, atmosphere and processing.

The second step uses the residual vectors after the Helmert transformation to derive local corrections in the chromatic a–b plane via inverse distance weighting. This step reduces nonlinear effects locally around the calibration colours and acts as a final fine-tuning step for chromaticity.

Overall, the proposed approach offers a practical way to improve visual consistency and colour stability in high-altitude aerial imagery using a single, large multi-colour ground target. The questionary showed that professional users of aerial imagery prefer true-to-life colours over radiometrically correct images. By collaborating closely with users, reference images perceived as natural or lifelike can be established. These lifelike images can then be analysed in relation to large colour patches measured with spectrometers. This approach allows documentation of users preferences regarding colour representation in aerial imagery and enables reproducibility to other locations. This approach has the potential to enhances radiometric stability in the construction of a nationwide orthophoto mosaic. However, it does not provide a full physical atmospheric correction to surface reflectance, and luminance-related effects remain only partially addressed.

5.1 Outlook

The experience so far has been that calibration surfaces of the size required are not practical to use in routine projects due to the necessary physical size and logistics. One observation is that the radiometric properties of certain satellite products appear to be more stable over time than those of aerial projects conducted in various European countries. This may have the potential to stabilise radiometric accuracy in aerial image campaigns, for example by using satellite-derived reflectance products as an external reference, either directly or via cross-calibration.

Future work will therefore explore strategies that combine ground targets, empirical image-based normalisation and external references such as satellite imagery or ground-based sensor networks. In addition, systematic evaluation of alternative local correction models (e.g. Gaussian process regression or polynomial mappings) and analysis of performance away from the target location will be important to assess the robustness and scalability of the proposed approach.

6. Acknowledgements

The authors would like to acknowledge Geovekst, a national collaboration for the establishment, and management of geographic information i Norway. Geovekst financed the large ground colour target used in this study.

We also thank Steinar Kjellevik Karlsen and Pål Tanem for their administration and logistical support during the fieldwork related to the ground colour target.

References

Ban, S., Kim, T., 2021. Automated reflectance target detection for automated vicarious radiometric correction of UAV images. *The International Archives of the Photogrammetry, Remote Sensing and Spatial Information Sciences*, 43, 133–137.

Bouvet, M., Thome, K., Berthelot, B., Bialek, A., Czapla-Myers, J., Fox, N. P., Goryl, P., Henry, P., Ma, L., Marcq, S. et al., 2019. RadCalNet: A radiometric calibration network for Earth observing imagers operating in the visible to shortwave infrared spectral range. *Remote Sensing*, 11(20), 2401.

Callieco, F., Dell'Acqua, F., 2011. A comparison between two radiative transfer models for atmospheric correction over a wide range of wavelengths. *International journal of remote sensing*, 32(5), 1357–1370.

Cantrell, S. J., Christopherson, J., 2024. Joint agency commercial imagery evaluation (jacie) best practices for remote sensing system evaluation and reporting. Technical report, US Geological Survey.

Chandelier, L., Martinoty, G. et al., 2009. Radiometric aerial triangulation for the equalization of digital aerial images and orthoimages. *Photogramm. Eng. Remote Sens*, 75(2), 193–200.

Chavez Jr, P. S., 1988. An improved dark-object subtraction technique for atmospheric scattering correction of multispectral data. *Remote sensing of environment*, 24(3), 459–479.

Collings, S., Caccetta, P., Campbell, N., Wu, X., 2011. Empirical models for radiometric calibration of digital aerial frame mosaics. *IEEE Transactions on Geoscience and Remote Sensing*, 49(7), 2573–2588.

Field Geospatial AS, 2025. Field Geospatial AS — Contact Page. `https://fieldgeo.com/contact/`. Accessed: 2025-11-06.

Geoforum, 2024. Geomatikkdagene lillehammer norway 2024. `https://geoforum.no/`. Accessed: 2025-11-16.

Honkavaara, E., Khoramshahi, E., 2018. Radiometric correction of close-range spectral image blocks captured using an unmanned aerial vehicle with a radiometric block adjustment. *Remote Sensing*, 10(2), 256.

McCamy, C. S., Marcus, H., Davidson, J. G. et al., 1976. A color-rendition chart. *J. App. Photog. Eng*, 2(3), 95–99.

Oliver, M. A., Webster, R., 1990. Kriging: a method of interpolation for geographical information systems. *International Journal of Geographical Information System*, 4(3), 313–332.

Richter, R., Bachmann, M., Dorigo, W., Muller, A., 2006. Influence of the adjacency effect on ground reflectance measurements. *IEEE Geoscience and Remote Sensing Letters*, 3(4), 565–569.

Shin, J. I., Cho, Y. M., Lee, H. M., Lim, P. C., Kim, T., 2020. A ground reference target detection method for automatic vicarious calibration of uav multispectral image. *40th Asian Conference on Remote Sensing: Progress of Remote Sensing Technology for Smart Future, ACRS 2019*.

Smith, G. M., Milton, E. J., 1999. The use of the empirical line method to calibrate remotely sensed data to reflectance. *International Journal of remote sensing*, 20(13), 2653–2662.

Variable, Inc., 2022. Spectro 1 pro. `https://variableinc.com/product/spectro-1-pro-affordable-precision-spectrophotometer/`. Accessed: 2026-05-18.

Vermote, E. F., Tanré, D., Deuze, J. L., Herman, M., Morcette, J.-J., 1997. Second simulation of the satellite signal in the solar spectrum, 6S: An overview. *IEEE transactions on geoscience and remote sensing*, 35(3), 675–686.

Wasmeier, P., 2025. Geodetic transformations. `https://se.mathworks.com/matlabcentral/fileexchange/9696-geodetic-transformations`. MATLAB Central File Exchange. Retrieved October 28, 2025.

Wilson, R. T., 2013. Py6S: A Python interface to the 6S radiative transfer model. *Computers & Geosciences*, 51, 166–171.